Article:
Burkle, D, De Motte, R, Taleb, W et al. (5 more authors) (2016) Development of an electrochemically integrated SR-GIXRD flow cell to study FeCO3 formation kinetics. Review of Scientific Instruments, 87 (10). 105125. ISSN 0034-6748

https://doi.org/10.1063/1.4965971

Development of an electrochemically integrated SR-GIXRD flow cell to study $FeCO_3$ formation kinetics

D. Burkle,[1a)] R. De Motte,[1] W. Taleb,[1] A. Kleppe,[2] T. Comyn,[3] S. M. Vargas,[4] A. Neville,[1] and R. Barker,[1]

[1]Institue of Functional Surfaces, University of Leeds, Leeds, LS2 9JT, United Kingdom
[2]Diamond Light Source Ltd, Diamond House, Didcot, Oxfordshire, OX11 ODE United Kingdom
[3]Ionix Advanced Technologies, 3M Buckley Innovation Centre, Firth Street, Huddersfield, HD1 3BD, United Kingdom
[4]BP America, Inc., Houston, Texas 77079

An electrochemically integrated Synchrotron Radiation-Grazing Incidence X-Ray Diffraction (SR-GIXRD) flow cell for studying corrosion product formation on carbon steel in carbon dioxide (CO_2)-containing brines typical of oil and gas production has been developed. The system is capable of generating flow velocities of up to 2 m/s at temperatures in excess of 80°C during SR-GIXRD measurements of the steel surface, enabling flow to be maintained over the course of the experiment while diffraction patterns are being collected. The design of the flow cell is presented, along with electrochemical and diffraction pattern transients collected from an initial experiment which examined the precipitation of $FeCO_3$ onto X65 carbon steel in a CO_2-saturated 3.5 wt.% NaCl brine at 80°C and 0.1 m/s. The flow cell is used to follow the nucleation and growth kinetics of $FeCO_3$ using SR-GIXRD linked to the simultaneous electrochemical response of the steel surface which were collected in the form of Linear Polarisation Resistance (LPR) measurements to decipher in situ corrosion rates. The results show that $FeCO_3$ nucleation could be detected consistently and well before its inhibitive effect on the general corrosion rate of the system. In situ measurements are compared with ex situ Scanning Electron Microscopy (SEM) observations showing the development of an $FeCO_3$ layer on the corroding steel surface over time confirming the in situ interpretations. The results presented demonstrate that under the specific conditions evaluated, $FeCO_3$ was the only crystalline phase to form in the system, with no crystalline precursors being apparent. The numerous capabilities of the flow cell are highlighted and presented in this paper.

I. INTRODUCTION

One of the most prevalent forms of internal corrosion when transporting oil and gas through carbon steel pipework is that associated with CO_2 corrosion [1]. During oil and gas production, $FeCO_3$ is one of the main corrosion products found on the internal walls carbon steel pipelines and piping systems. This growth of $FeCO_3$ is of importance in CO_2 corrosion due to its influence on the corrosion rate when covering the corroding surface [2-4]. Under specific operating conditions, a highly dense, protective $FeCO_3$ film is formed. The high degree of protection is attributed to a combination of a surface blocking effect from the precipitated crystals as well as $FeCO_3$ presenting itself as a diffusion barrier to electrochemically active species involved in the charge-transfer process as the layer becomes denser and less porous. The transient corrosion rate behaviour of carbon steel during $FeCO_3$ formation and the magnitude of the steady state corrosion rate after film formation is dictated by the crystal layer nucleation, growth, morphology and its stability/resistance against chemical/mechanical removal [5-8]. Therefore, understanding the factors governing the rate of formation of $FeCO_3$ on the corroding surface of mild steel is an important step in understanding the overall CO_2 corrosion process. Accounting for $FeCO_3$ formation (and the formation of other corrosion products, for that matter) on the internal walls of carbon steel pipework is crucial when developing an accurate corrosion prediction model or when developing a robust corrosion management strategy. It is important to understand which corrosion products are formed and to what extent their rate of formation, morphology and protectiveness are influenced by changes in the operating conditions and the environment. However, two main

a) Danny Burkle. Electronic mail: mn09d2b@leeds.ac.uk.

challenges present themselves when analysing corrosion product film formation processes in oil and gas environments:

i. It is difficult to determine $FeCO_3$ growth kinetics on the steel surface during formation without stopping experiments and performing mass gain measurements to identify the quantity of $FeCO_3$ on the steel surface.
ii. Due to the rapid formation of $FeCO_3$ in a supersaturated brine, is difficult to capture the very early nucleation and growth kinetics without using in situ monitoring techniques that offer real-time kinetic information.

To address the aforementioned challenges, several research groups have already exploited in situ SR-GIXRD for determining the nature of corrosion products in CO_2 corrosive environments [9-13]. The use of in situ SR-GIXRD offers key information relating to the composition and orientation of any crystalline material being formed in the presence of an electrolyte in realistic conditions with real-time relative kinetic information during the early stages of formation [14]. This eliminates the possible oxidation of surface corrosion products as a result of the removal process from the vessel/solution which will potentially lead to incorrect conclusions to be drawn in relation to the film formation process. Researchers have reported that in simple CO_2-containing brine solutions a number of iron oxides/hydroxide phases to form in conjunction with $FeCO_3$. Such phases include magnetite (Fe_3O_4) [15, 16], chukanovite ($Fe_2(OH)_2CO_3$) [9-13], wustite (FeO) [13] and goethite (FeO(OH)) [13]. However, these studies have either been performed in oxygen contaminated systems (as suggested by the authors themselves) [16], or the growth of the corrosion product was accelerated by applying excessive currents/voltages to the sample under study [11, 12] which were not realistic of the actual corrosion kinetics encountered in the field.

To overcome these limitations, a new methodology and cell design is proposed in this work which enables corrosion rates and film formation/characteristics to be measured simultaneously without exposure of the sample to oxygen in a naturally corroding flowing cell. Typically, the use of in situ synchrotron radiation in the characterisation of electrochemical systems requires the design of a cell to carry out electrochemistry whilst facilitating X-ray measurement. There are a number of examples in the literature of in situ SR-GIXRD studies using a variety of electrochemical cells designs [11, 13, 17-19], each of which can carry out a wide variety of in situ X-ray studies. De Marco and Veder [19] reveal many electrochemical-cell designs during an extensive review and assessment of the literature available on this topic. The work presented here describes the development of a new and unique SR-GIXRD flow cell integrated with in situ electrochemical capabilities which is utilised to measure and understand the nucleation and growth of $FeCO_3$ as well as other species which may also form during the corrosion process on a naturally corroding surface. The early nucleation and growth kinetics of $FeCO_3$ of a naturally corroding surface in a flowing, deaerated system are characterised in situ for the first time. In situ results were then confirmed using ex situ SEM analysis of the carbon steel surface and the morphology of the corrosion product layer that formed.

II. SR-GIXRD FLOW CELL DESIGN

The SR-GIXRD flow cell is integrated with in situ electrochemistry and is capable of generating flow velocities up to 2 m/s at temperatures in excess of 80˚C. Diffraction patterns can be collected through water, enabling the flow to be maintained over the course of the experiment while data is collected in real time and correlated with electrochemical measurements. The design of the flow cell is shown in Figure 1 and comprises two main components (the flow cell base (4) and a top plate (1)) machined from Acetal that are mounted together with M5 socket cap stainless steel screws (8). A groove was machined into the base of the cell to accommodate a custom Viton O-ring (11) to facilitate an air-tight seal. The top plate has a section machined out to accommodate a 125 µm thick Kapton® window (2) to enable X-ray transmittance.

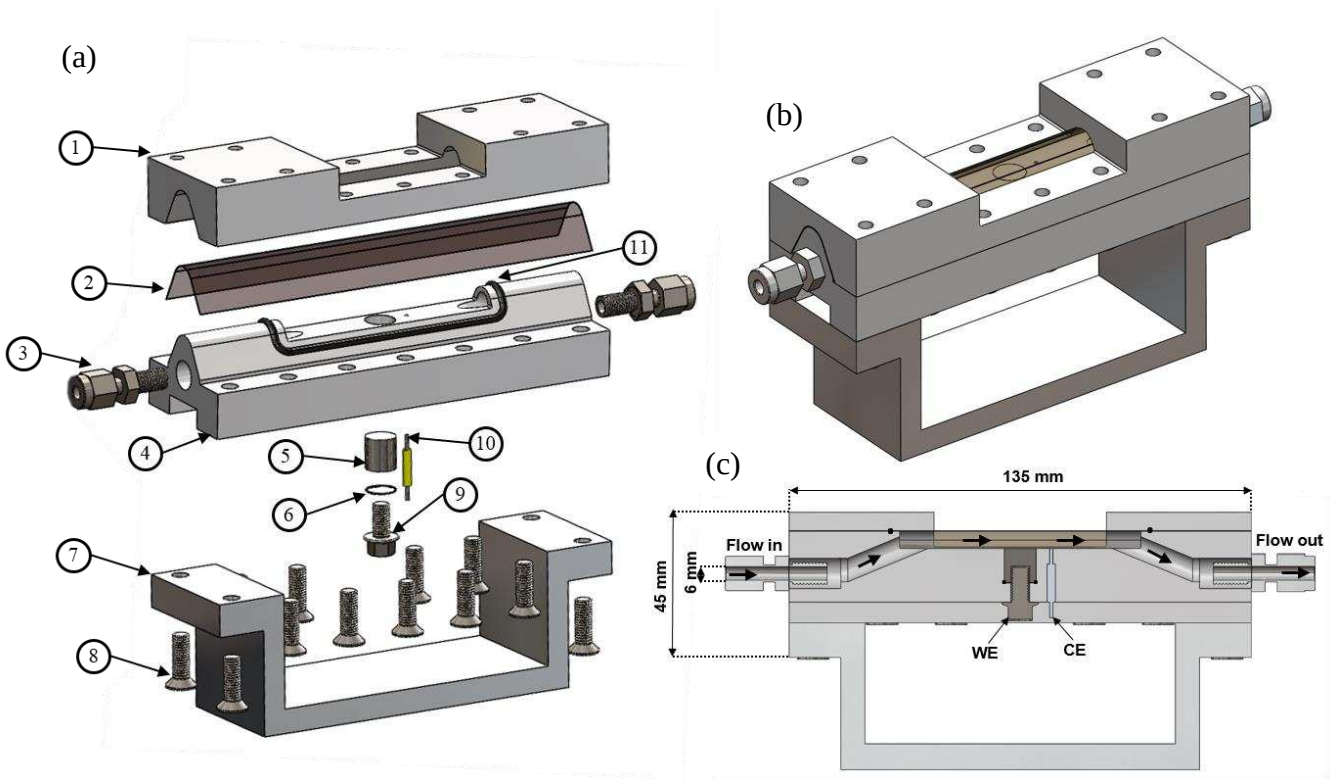

Figure 1. 3D schematic diagrams of the SR-GIXRD cell: (a) Exploded assembly of individual components; (b) Assembled view; (c) Schematic cross section; (WE = working electrode), (CE = counter electrode).

A 9 mm diameter (and 9 mm in length) cylindrical X65 grade carbon steel sample (5) was embedded into the base of the flow cell and flush mounted with the top surface of the base plate. The steel sample acted as the working electrode (WE) in the three-electrode cell used to acquire electrochemical responses. The carbon steel sample was machined to allow a threaded M5 bolt (9) to be positioned into the base, providing both electrical contact but also acting with a Viton O-ring (6) to provide a compression seal when tightened, securing the sample into the base plate and preventing oxygen ingress. The substrate surface height position was highly reproducible between experiments minimising requirements for realignment between each experiment. This is an important design feature, which ensured that the maximum amount of beam time was used for data collection and not cell alignment. The tubing used to complete the flow loop was a ¼" stainless steel flexi-tube hose (9.14 mm outer diameter) with a PTFE inner bore (6 mm inner diameter) to minimise $FeCO_3$ precipitation elsewhere in the system. Stainless steel Swagelok male tube connecters (3) were used for the flow inlet and outlet. The electrochemical set-up used for the flow cell design was a standard three-electrode cell (see Figure 2) which comprised of the X65 grade carbon steel sample as the WE, a 1 mm in diameter 99.9% pure platinum rod (10) as the counter electrode (CE) (which is also flush mounted with the surface 3 mm away from the WE) and a Ag/AgCl reference electrode (RE) positioned downstream in a separate port system.

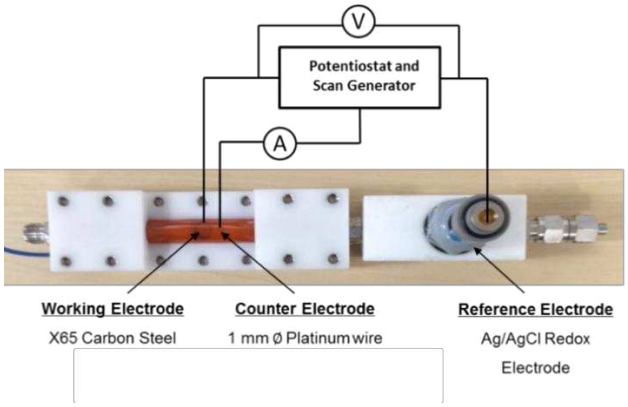

Figure 2. Flow cell electrochemical set-up used during SR-GIXRD tests: Three-electrode set-up.

III. SYNCHROTRON EXPERIMENTAL PROCEDURE

A. Experimental set-up and sample preparation

Figure 3 shows a schematic of the flow cell set-up at beamline I15, Diamond Light Source, Oxfordshire as well as an image taken in the experimental hutch. To demonstrate the capabilities of the flow cell, one particular experiment is highlighted in this work. The following paragraphs provide information pertaining to the experimental approach and the test conditions evaluated.

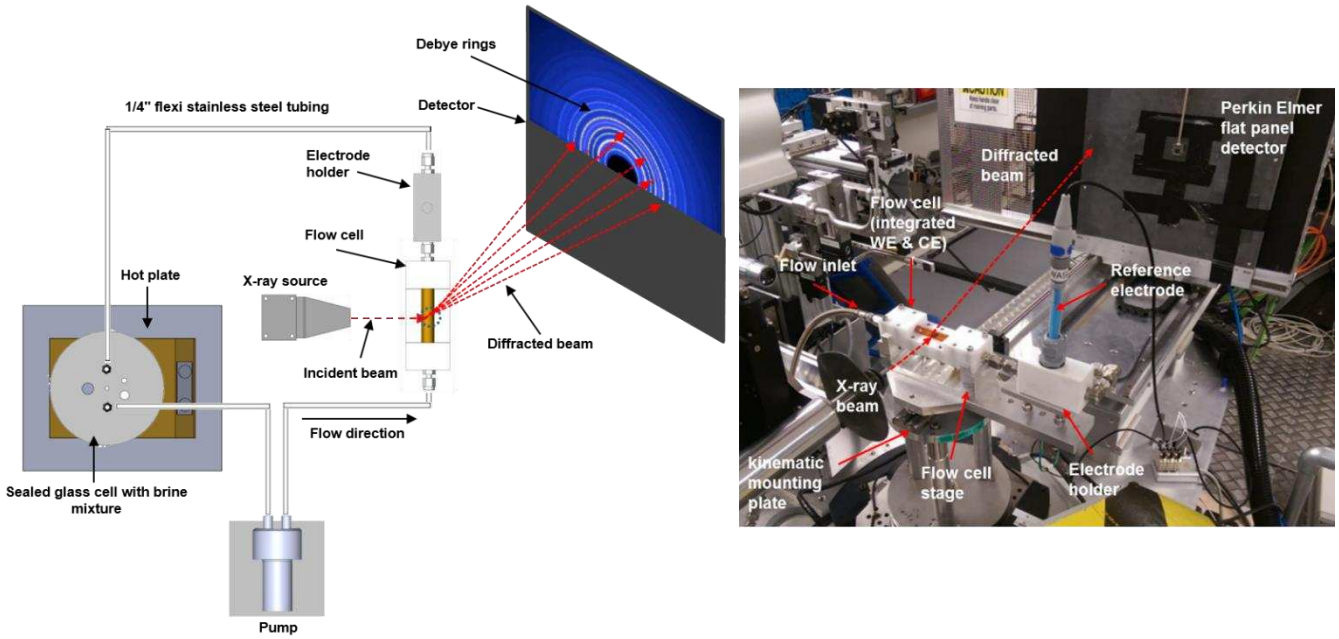

Figure 3. The cell set-up during Synchrotron tests: Photograph (right) and schematic (left) of the flow cell set-up used on the Diamond Light Source beamline (I15).

A formulated saline solution circulates within a closed loop between the flow cell and a locally heated 1 litre vessel via the use of a centrifugal micro-pump to provide precise flow rate control. The flow velocity of the test was maintained in a laminar flow regime at 0.1 m/s for the experiment discussed here (although much higher velocities up to 2 m/s are possible which would prove advantageous in studies involving mechanical/chemical dissolution or mass-transfer controlled precipitation process) and was controlled using a customised magnetic drive gear micro-pump (Micropump® Series GJ-N23) which offers high precision control. The 1 litre vessel was continuously

sparged with CO_2 throughout the experiment to ensure the solution was completely saturated. Prior to the start of the experiment, the test sample was wet ground up to 600 silicon grit paper, degreased with acetone, rinsed with distilled water and dried with compressed air. The sample was then positioned into the base of the flow cell and electrical wires were connected to the steel samples prior to alignment. The composition of the steel is provided in Table I. A sample surface area of 0.64 cm^2 was exposed to the electrolyte once fluid flow was initiated through the cell. The experiment considered here was performed for 4 hours with in situ electrochemical measurement and SR-GIXRD measurements being collected throughout the duration of the test. The flow cell was bolted flat onto a specially designed stage that was attached to a kinematic mounting plate. This allowed the flow cell to be easily removed from the stage while fully assembled so that dismantling and cleaning parts and the removal of the sample could be performed in a laboratory away from the beamline. Once flow was initiated, electrochemical and X-ray diffraction measurements commenced after a period of no more than 3-4 minutes.

TABLE I. Composition of X65 pipeline carbon steel (wt.%)

C	Mn	Ni	Nb	Mo	Si	V	P	S	Fe
0.15	1.422	0.09	0.054	0.17	0.22	0.06	0.025	0.002	97.81

B. Brine preparation

The experiment was conducted in a de-aerated 3.5 wt.% NaCl brine saturated with CO_2, representing oil and gas production environments. CO_2 was bubbled into the system for at least 4 hours prior to the experiment and throughout the duration of the experiment which was conducted at atmospheric pressure. The temperature of the solution was maintained at 80°C using a high power Carousel Tech Stirring Hotplate with in integrated Pt1000 stainless steel temperature sensor that was immersed into the 1 litre vessel through an oil filled glass tube. The pH of the solution was adjusted to ~6.8 and was controlled by adding sodium bicarbonate (8g $NaHCO_3$ per 1 litre solution). The temperature drop between the hotplate and the flow cell was less than 1ºC.

C. In situ electrochemical measurements

Electrochemical measurements were conducted using an ACM Gill AC potentiostat in order to determine the in situ corrosion rate of the X65 carbon steel working electrode. Linear polarisation resistance (LPR) measurements were performed by polarising the sample ±15 mV vs. the open circuit potential (OCP) at a scan rate of 0.25 mV/s to obtain a polarisation resistance (R_p). LPR measurements were undertaken every 5 minutes, allowing the sample to remain at OCP between each reading. Tafel polarisation measurements were completed using new and wet ground samples in separate experiments by performing anodic and cathodic sweeps starting at OCP and scanning to +150 mV or -500 mV vs. OCP, at a scan rate of 0.5 mV/s. Anodic and cathodic sweeps were performed separately in a different experiment and the determined Tafel constants were used to determine an appropriate Stern-Geary coefficient to provide a more accurate calculation of corrosion rates. Solution resistance was measured using AC impedance and the polarisation resistance values were then corrected to give the charge-transfer resistance. Once the Stern-Geary coefficient was established, it was then used in combination with Faraday's Law and the measured values of charge transfer resistance to estimate the general corrosion rate of the system.

D. In situ SR-GIXRD measurements

The in situ SR-GIXRD experiments were conducted at beamline I15 at the Diamond Light Source, UK. The beamline provides monochromatic high-energy X-rays from 20 to 80 keV in combination with a small beam spot size down to <20 μm which can penetrate into complex sample assemblies permitting detailed mapping of structural order or disorder and chemical composition [20]. High energies (compared to conventional XRD) are required to

penetrate through the water (~15 mm path length) in the flow cell and the beam size allows scanning of the samples with appropriate spatial resolution. The X-ray beam energy in these experiments was 40 keV (i.e. $\lambda = 0.3099$ Å) and the beam size was 70 µm in diameter. The incident-beam to sample angle was set to 4º and in situ SR-GIXRD measurements over the range of 2θ=0-12° were collected continuously during the experiments. Using 40 keV radiation along with an incident angle of 4º, the penetration depth of the beam in to the steel sample was calculated using PANalytical's HighScore plus software. The estimated penetration depth using these values was 55µm. Before switching the pump on, a dry scan of the steel sample was taken to use as baseline data relative to the in situ data and to check the alignment of the beam. Data acquisition then began 3-4 minutes after the pump was switched on. This was the time taken to carry out the required safety checks and closure of the experimental hutch before the beamline shutter was opened. Individual data sets were collected for 60 seconds at any given location. In order to maximise the accuracy of the extent of crystal growth, a loop was devised to scan five measurements across a 2 mm path located at the centre of the sample to ensure more reliable statistics if the film formed was non-uniform across the steel surface. Therefore the overall scanning time to complete one cycle of the surface was 5 minutes. The diffraction results in this paper show the average of the five scanned locations to represent a larger proportion of the overall surface as well as the individual transients themselves. The flux available at I15, together with the fast data collection times of 60 seconds enables intermediate phases (if any) to be measured. Diffraction images were recorded using a Perkin Elmer flat panel detector located 975 mm from the sample and conventional 2θ diffraction patterns were generated by radial integration of the Debye rings using the software Fit2D with subsequent data analysis performed by profile fitting and Rietveld analysis.

IV. SYNCHROTRON EXPERIMENT RESULTS

The experimental work enabled corrosion kinetics and in situ electrochemical responses to be related to diffraction measurements in a flowing cell in a naturally corroding CO_2 system. Allowing the steel to corrode at OCP is crucial when describing the formation process of $FeCO_3$. Under forced conditions as described previously, the growth of the corrosion product layer formed does not represent the true nature of the process. In order to ensure the growth of $FeCO_3$ (or any other phases present) the corrosion kinetics were enhanced using a high temperature and high pH at a low flow velocity, making the conditions more favourable for formation.

A. Flow Cell Performance: Electrochemical observations

Figure 4(a) shows the graph indicating the in situ electrochemical measurements of the corrosion rate and OCP verses time for a 240 minute test conducted on a naturally corroding sample under the conditions described previously. The corrosion rate of the system at the start of the test is ~2 mm/year which increases to ~2.15 mm/year throughout the first 60 minutes of the test until a semi-protective $FeCO_3$ layer has formed, blocking active steel sites available for dissolution causing the corrosion rate to decrease with time. The corrosion rate drops to a value of ~0.54 mm/year after 240 mins as a result of $FeCO_3$ covering the majority of the steel surface. Figure 4(b) shows the Tafel plots obtained by performing separate anodic and cathodic sweeps once the corrosion rate had stabilised at 0.1 mm/year after 12 hours of testing during off beamline tests. The measured corrosion rate from the synchrotron test were calculated based on these measured Tafel constants. The anodic Tafel slope (βa) measured ~60 mV/decade which is in good agreement with literature at similar operating temperatures [21]. However, βc proved difficult to measure due to interference from high anodic currents at low negative overpotentials influencing the Tafel behavior. However the cathodic Tafel slope (βc) for CO_2-systems is well characterised by Nesic, et al. [21] to be ~120 mV/decade which was implemented to give Stern-Geary coefficient (S.G) of 17.

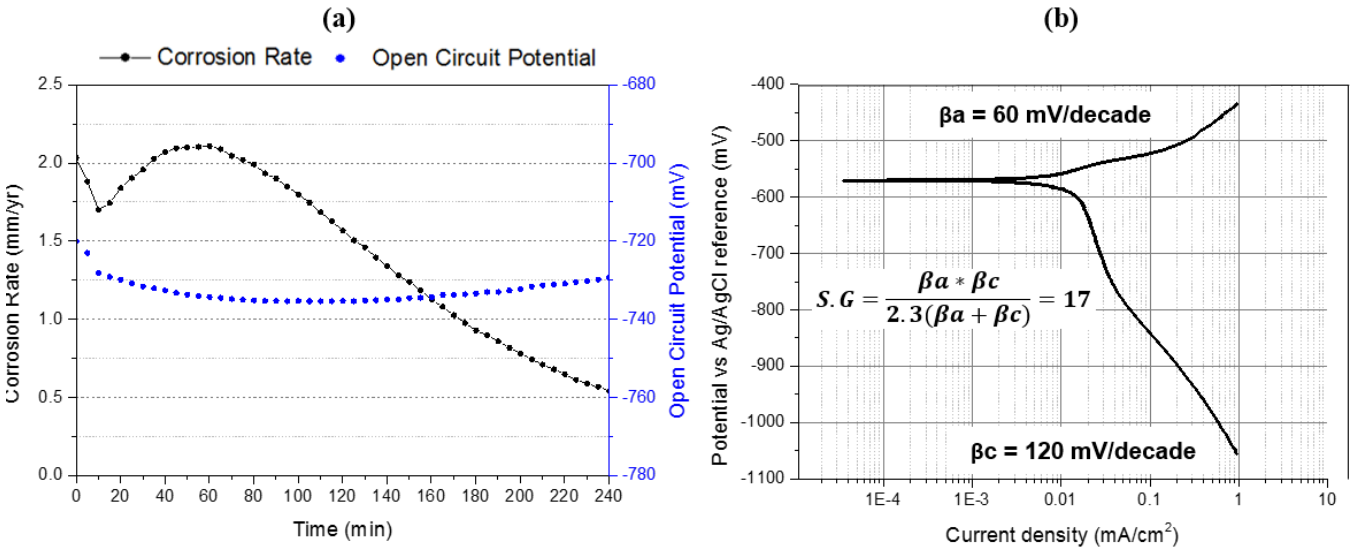

Figure 4. In situ electrochemical data: a) Corrosion rate and open circuit potential data collected at Diamond Light Source beam line (I15); b) Tafel plots for X65 carbon steel samples ran in-house under the identical conditions to SR-GIXRD tests after 12 hours (Note: Increase in potential is due to pseudo-polarisation of the sample [15]); (S.G = Stern-Geary coefficient), (βa = Anodic Tafel slope), (βc = Cathodic Tafel slope).

B. Flow Cell Performance: X-Ray Diffraction Results

In situ SR-GIXRD data over the range 2θ=0-12° was collected continuously for 240 minutes. Figure 5 shows a plot of multiple patterns representing the intensity against 2θ showing the growth of the phases present over time (patterns are offset for clarity). Each pattern represents the cumulative sum of all five scans across the sample at each time interval reflecting the intensity of the phases present across a 2 mm linear region. Phase identification of the in situ SR-GIXRD patterns reveals that the only crystalline phase detected on the steel surface during the test was $FeCO_3$. Iron carbide (Fe_3C) was present prior to running the tests and was a part of the steel composition. Throughout the duration of the entire experiment, the growth of the crystals was dominated by the growth of the plane observed at 2θ=~6.35º (Miller Index – [104]). The growth and shape of the major $FeCO_3$ plane is illustrated by the boxed area in Figure 5 and in the magnified image provided in Figure 6(a). Figure 6(b) shows the growth of the major $FeCO_3$ plane [104] at each location scanned across the sample and shows that crystalline $FeCO_3$ was detected at each location on the sample within 7-15 minutes of scanning. The major $FeCO_3$ crystal plane at each of the five locations scanned shows a similar (but not identical) growth trend with marginally different characteristics (emergence time, growth rate, final intensity) indicating heterogeneous growth across the surface of the sample. The growth mechanism is depicted more clearly from the cumulative intensity of all five points over the steel surface and is presented in Figure 7. In situ measurements are compared with ex situ SEM observations showing the development of an $FeCO_3$ layer on the corroding steel surface which is shown in Figures 7(a-e). The SEM images (Figures 7(a-d)) are analysed at a magnification of x3000 to project an area of ~70x70 µm to represent the size of the beam and to illustrate the area of the surface being scanned at each location. Furthermore, Figure 7(e) shows the kinetics of the $FeCO_3$ layer in the form of the cumulative intensity from all five points providing an average over the steel surface and can be compared with the electrochemical response which is also an average corrosion rate over the steel surface. From the accumulated measured intensity, three steps characterise the growth mechanism: (1) An induction time when the measured intensity is zero (from 0 to the 7th minute); (2) Nucleation of the $FeCO_3$ crystals (between the 7th and 14th minute); (3) Nucleation-growth stage which is characterised by an increase of the growth according two different regimes; the growth rate first rapidly increases (between the 14th and 175th minute) and then slows down towards the end of the experiment (240th minute).

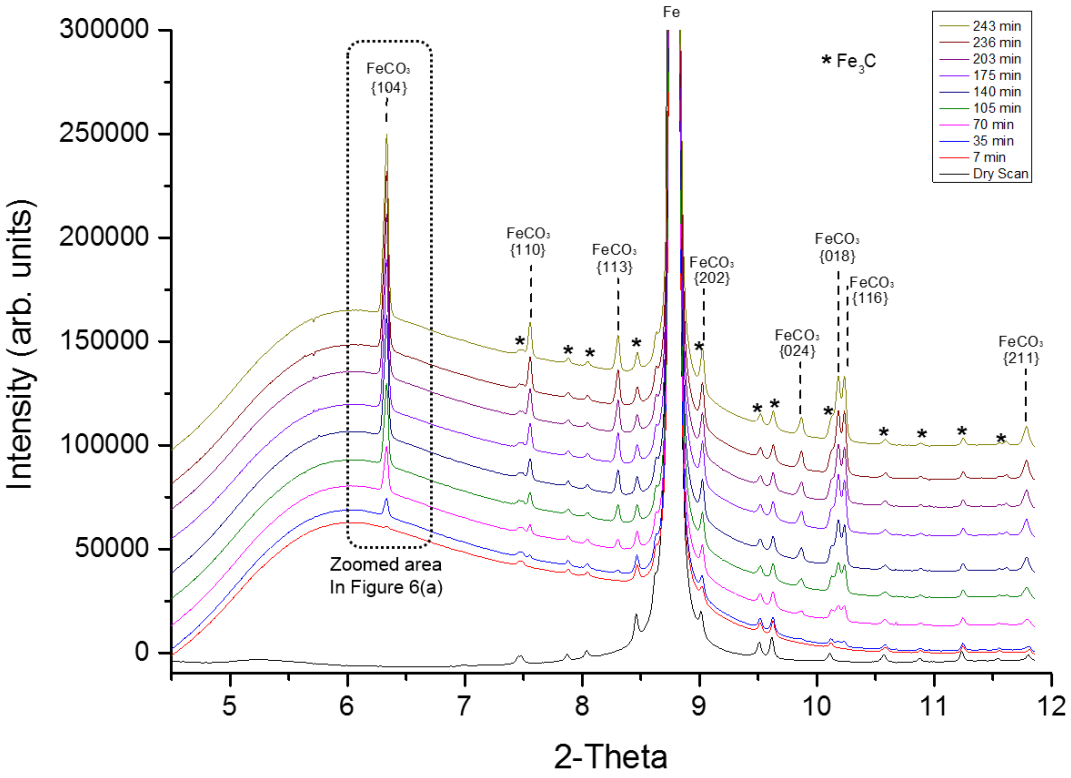

Figure 5. Selection of in situ diffraction patterns recorded as a function of time at the Diamond Light Source powder diffraction beam line (I15). Each plot represents the phases present across a 2 mm path at the centre of the sample.

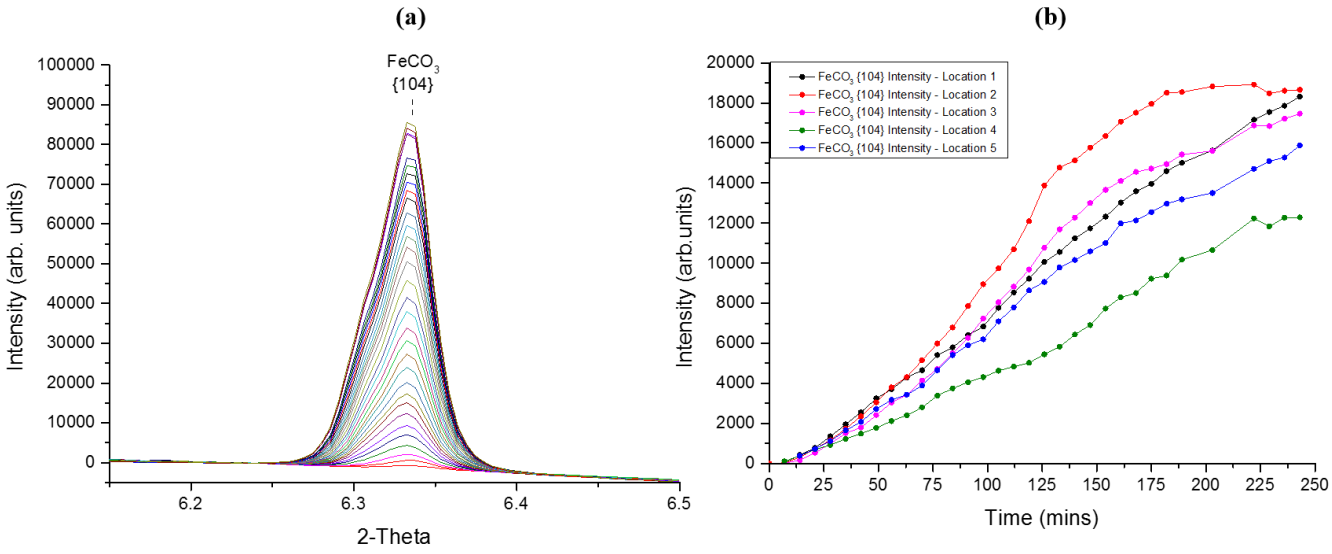

Figure 6. In situ diffraction patterns recorded over time at the Diamond Light Source beam line (I15) (a) Diffraction patterns ~every 7 minutes; (b) Diffraction patterns for major $FeCO_3$ peak over time for each of the 5 scans performed over a 2 mm line scan.

After the induction time (7 minutes), the major $FeCO_3$ peak intensity begins to increase due to the crystals forming on the steel surface through heterogeneous nucleation. After 30 minutes, following nucleation, the crystals on the

surface begin to grow with crystal sizes varying from <1 μm to 2 μm in width (Figure 7(a)). At this stage the crystals offer little or no protection against corrosion. After 60 minutes, the nucleated crystals have grown with an average size from 1 μm to 5 μm in width (Figure 7(b)) whilst new crystals continue to nucleate on to the steel surface. In conjunction with this behaviour, the corrosion rate begins to decrease as a result of the $FeCO_3$ crystals blocking active sites on the steel surface. From 60 minutes onwards, the combined in situ observations and ex situ SEM images exemplify that this process of nucleation and growth continues until the $FeCO_3$ film has the ability to reduce the corrosion rate significantly. This sequence of nucleation and growth illustrates that as the $FeCO_3$ layer develops, larger proportions of the surface are being covered with crystals and ultimately reducing the reaction rate of species across the entire surface (i.e. production of Fe^{2+}) which has a direct impact on the formation of $FeCO_3$, reducing the precipitation rate and therefore less $FeCO_3$ is formed. Therefore, as the $FeCO_3$ layer builds up, the precipitation kinetics slow down which is captured by the SR-GIXRD measurements after 175 minutes. After 240 minutes, further nucleation and growth then contributed to a subsequent buildup of the $FeCO_3$ layer with crystals ranging from 1 μm to 10 μm.

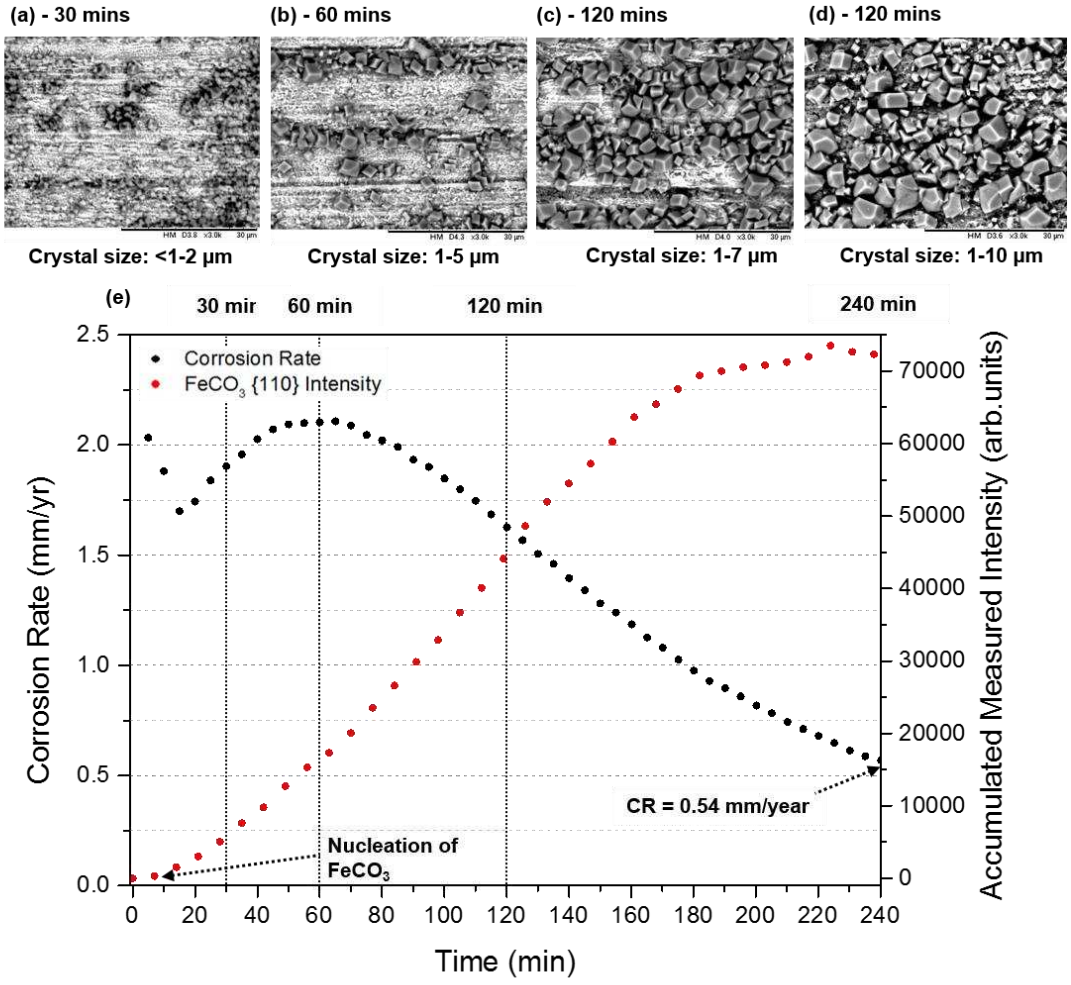

Figure 7. Development of the $FeCO_3$ crystals (a)-(d) SEM images over time; (e) In situ corrosion rate and major $FeCO_3$ plane intensity verses time.

This work has demonstrated that the flow cell can be used for in situ SR-GIXRD studies of scale formation on mild steel surfaces that are naturally corroding in a corrosive and flowing system. The results suggest that there is a qualitative relationship between the corrosion rate and the $FeCO_3$ intensity, and that further analysis (and focus of

the future work) is to be able to establish a quantitative relationship (in terms of mass gain, film thickness and surface coverage) to help further determine precipitation kinetics.

V. CONCLUSIONS

A new system comprising of a flow cell with integrated in situ electrochemistry and SR-GIXRD capabilities has been developed to facilitate corrosion measurements under a variety of experimental conditions. Some of the first data obtained for in situ analysis has been presented to show the capabilities of the cell. Using in situ SR-GIXRD, the formation of corrosion products on a naturally corroding carbon steel sample in a CO_2 saturated brine has been followed as a function of time in a flowing cell. The results have shown that $FeCO_3$ nucleation could be detected consistently and well before its inhibitive effect on general corrosion rate was recorded from electrochemical responses. The results presented also demonstrate that under the specific conditions evaluated, $FeCO_3$ was the only crystalline phase to form in the system, with no crystalline precursors being apparent prior to or during its formation. The $FeCO_3$ intensity plots of the most prominent peak at each of the locations scanned shows a nucleation period, followed by a growth stage. The major $FeCO_3$ crystal plane at each of the five locations scanned shows surface growth is heterogeneous (i.e. non-uniform), highlighting the importance of multiple scans to accumulate a clear interpretation of the growth kinetics across the steel surface. However, a cumulative intensity relationship with corrosion rate and film formation is also apparent. The system opens up several avenues of research where real-time corrosion measurements might enable some mechanisms to be determined. The flow cell will be used in future investigations into the effect of different environmental parameters on the formation of $FeCO_3$. Future work will also focus on establishing a quantitative relationship with the measured intensities.

ACKNOWLEDGMENTS

We would like to thank the Diamond Light Source for beam time (Beamline I15, reference EE12481-1), specifically Dr. Annette Kleppe and Allan Ross for assistance before and during our visit. We would also like to thank Steve Caddick, Graham Brown and Mick Huggan for their expertise and assistance with the design and manufacture of the flow cell.

REFERENCES

[1] S. Papavinasam, Chapter 4 - The Main Environmental Factors Influencing Corrosion, In Corrosion Control in the Oil and Gas Industry, 179 (2014).
[2] M. H. Nazari, S. R. Allahkaram, M. B. Kermani, Materials & Design, 31, 7, 3559 (2010).
[3] M. B. Kermani, A. Morshed, CORROSION, 59, 8, 659 (2003).
[4] L. S. Moiseeva, Protection of Metals, 41, 1, 76 (2005).
[5] C. de Waard, U. Lotz, A. Dugstad, CORROSION, 128, (1995).
[6] S. Nesic, L. Lunde, CORROSION, 50, 9, 717, (1994).
[7] F. Pessu, R. Barker, A. Neville, CORROSION, 71, 5, 1452 (2015).
[8] R. Barker, Y. Hua, A. Neville, International Materials Reviews, 1 (2016).
[9] R. De Marco, Z.T. Jiang, B. Pejcic, E. Poinen, J. Electrochem. Soc, 152, 10, B389 (2005).
[10] R. De Marco, Z.T. Jiang, D. John, M. Sercombe, B. Kinsella, Electrochimica Acta, 52, 11, 3746 (2007).
[11] B. Ingham, M. Ko, G. Kear, P. Kappen, N. Laycock, J. Kimpton, D. Williams, Corrosion Science, 52, 9, 3052 (2010).
[12] B. Ingham, M. Ko, N. Laycock, N. M. Kirby, D. E. William, Faraday Discussions, 180, 171 (2015).
[13] G. R. Joshi, J. Lapinski, O. Bikondoa, K. Cooper, D. L. Engelberg, M. G. Dowsett, R. Lindsay, NACE International, 5674 (2015).
[14] J. Robinson, F. C. Walsh, Corrosion Science, 35, 1-4, 791 (1993).

[15] J. Han, D. Young, H. Colijn, A. Tripathi, S. Nešić, Industrial & Engineering Chemistry Research, 48, 13, 6296 (2009).
[16] E. Chan, PhD thesis, Curtin University, Perth, Australia, (2011).
[17] N. A. S. Webster, I. C. Madsen, M. J. Loan, N. V. Y. Scarlett, K. S. Wallwork, Rev. of Sci. Inst., 80, (2009).
[18] T. Chen, A. Neville, K. Sorbie, Z. Zhong, Faraday Discussions, 136, 355 (2007).
[19] R. De Marco, JP. Veder, Trends in Analytical Chemistry, 29, 6, (2010).
[20] Diamond Light Source, Beamline I15. Available at: http://www.diamond.ac.uk/Beamlines/Engineering-and-Environment/I15-Extreme.html.
[21] S. Nesic, J. Postlethwaite, S. Olsen, Corrosion, 52, 4, 280 (1994).